

The effect of surface damage and residual stresses on the fatigue life of nickel superalloys at high temperature

R.M.N. Fleury^{a,*}, E. Salvati^b, D. Nowell^{b,c}, A.M. Korsunsky^b, F. Silva^d, Y.H. Tai^d

^a*Institute of Mechanics and Numerical Mechanics, Leibniz University Hannover, 30167 Hannover, Germany*

^b*Department of Engineering Science, University of Oxford, Parks Road, OX1 3PJ, Oxford, UK*

^c*Department of Mechanical Engineering, Imperial College London, SW7 2AZ, London, UK*

^d*Rolls-Royce plc, P.O. Box 31, DE24 8BJ, Derby, UK*

Abstract

A methodology for evaluating the effect of surface damage in the fatigue life of nickel superalloys is presented in this paper. Dents generated due to low velocity impacts of hard objects were simulated using a finite element (FE) model. The residual stress distribution underneath the dent root obtained numerically was compared with the measurements on experimentally simulated damaged specimens using ring-core milling at the micron scale through a combined Focused-Ion Beam and Digital Image Correlation technique (FIB-DIC). The numerical and experimental results for the residual stress show good agreement in terms of residual stress trends and magnitudes. The residual stress distribution obtained via the FE model was subsequently used in a fatigue short crack growth model for an estimation of the fatigue life of dented specimens. The fatigue life predictions were then compared with experimental fatigue results for the nickel superalloy at high temperatures. The comparison shows a significant improvement in the prediction of fatigue life of parts with superficial damage due to careful consideration of the residual stresses around the damage.

Keywords: surface damage; residual stress; fatigue; FIB-DIC; nickel superalloys

1. Introduction

Handling damage on the surface of components may occur during manufacturing, assembly and maintenance of aero-engines. Such damage is typically produced by low velocity impacts of

*Corresponding author.

Email address: rodolfo.fleury@eng.ox.ac.uk (R.M.N. Fleury)

hard objects, such as tools dropped on parts during servicing or parts colliding with each other during assembly, causing scratches and shallow dents on the surface. These surface damage marks are likely to affect the structural integrity of aero-engine components. Damage due to higher velocity impacts, such as foreign object damage (FOD) and domestic object damage (DOD), has been extensively studied over the past fifteen years [1–4]. In contrast to these higher velocity events, handling damage generally results from the impact of objects with higher mass at lower velocities. Despite the obvious differences between these problems, the consequences of the surface damage are very similar in terms of fatigue life. As pointed out by Mall et al. [5], the effect of surface damage on crack initiation and propagation is determined by a combination of three factors. These are the stress concentration due to the geometry of the damage mark, the residual stress field created, and the micro-structural changes by the deformation. Currently, crack propagation analysis of components with small scratches and dents is frequently carried out by assuming the damage geometry to be an initial crack of same length and depth. This approach is generally very conservative, since it takes into account neither the residual stress field generated near the damage nor the time that it takes for the crack to initiate from the stress concentrator.

The first step for developing a model which incorporates the competing factors around the damage is to reproduce in laboratory similar surface dents and scratches as those found in real components. The challenge of simulating in laboratory the conditions in which handling damage may occur have been discussed by previous authors [6, 7]. While the dent were created by indentation in [7] and previous work may be found suggesting that the residual stress field obtained by indentation is similar to that obtained by low velocity impacts [8], here, the experimental simulation of handling damage was carried by shooting onto the specimen a projectile with a blunt tip as to produce a dent similar to those observed in real engine components. This procedure is described in detail in [6] and the result is a more accurate representation of real engine occurrences of surface damage during manufacturing and maintenance of engines.

Another aspect of this study is with respect to the effect of the residual stresses generated around the dent when surface damage occurs. Doremus et al. [7] carried out a study on the effect of residual stresses around dents and scratches using Inconel 718 specimens. Their paper has shown that the number of cycles for crack initiation in dented specimens reduces when the residual

stresses are relaxed, in this case by thermal treatment, whereas scratches show the opposite effect. It has also been shown that crack initiation in samples with surface damage is influenced by the same three factors suggested in [5]. In the work of Gourdin et al. [9, 10], the effect of scratches and dents on crack initiation and propagation was assessed by using a potential drop technique. Thermal treatment of the samples was also carried out in order to evaluate the effect of the residual stress on the crack propagation, showing that the compressive residual stress under the dents significantly reduces the crack propagation.

Recently, the authors have conducted a series of work on handling surface damage. First, the characterisation of surface damage due to the impact of hard blunt objects was studied [6]. The work focused on the geometry of the dent created, i.e. dent depth as a function of the impact velocity, and on developing a modelling tool to predict the geometrical stress concentration produced by the damage and the residual stress field around it. The residual stresses generated during the impact were validated by comparing the FE results with the residual stresses measured by X-ray diffraction (XRD). A second paper examines the propagation of a crack under the dent and in the presence of the residual stress field [11]. A dislocation density approach [12, 13] is used to obtain the stress intensity factors of a crack propagating under the dent. A short crack propagation law first introduced by Oakley and Nowell [14] was used in the analysis and the difference in fatigue life for parts with different dent depths highlighted. One important conclusion in [11] was that residual stress relaxation mechanisms need to be taken into account in order to accurately predict the fatigue life of damaged specimens.

Although previous work on the subject have been able to characterise the damage and the residual stresses around it, comparison with fatigue experiment, particularly at high temperature, is still missing in the literature. Hence, the current paper aims to compare the fatigue life predictions with experimental results, for which is necessary to incorporate residual stress relaxation mechanisms into the fatigue life calculations. In order to validate the residual stresses obtained with the FE model along the crack path, the stresses along the crack path is needed, which in [6] was done only over a large averaging area using XRD. Therefore, a point-wise comparison of the residual stresses obtained from the FE model with experimentally measured results is also carried out by using the micro ring-core method, which is a combination of Focused-Ion Beam and Digital

Image Correlation techniques (FIB-DIC).

2. Experimental methodology

2.1. Experimental damage simulation

Low velocity impact tests were conducted on a modified split Hopkinson bar rig (Fig. 1a) at the University of Oxford. The experimental damage simulation was conducted on the flat face of RR1000 nickel superalloy fatigue test specimens with rectangular cross section. The specimens were mounted with their wider faces perpendicular to the striker bar and dents were created on both side of the specimen in order to avoid bending effects. A typical surface damage mark is illustrated in Fig. 1b. The geometry of the damage is similar to that of the indenter, which has a hardened steel ellipsoidal tip with two principal radii of curvature ($R_1 = 12.5$ mm and $R_2 = 1$ mm).

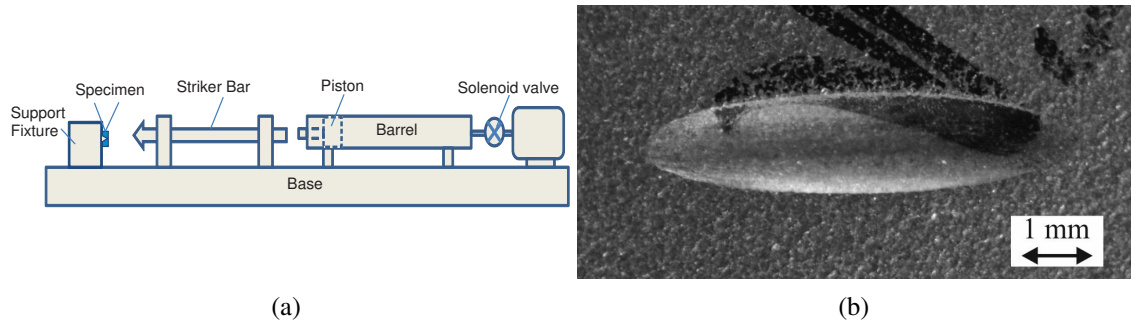


Figure 1: (a) Schematic representation of the modified Hopkinson bar used in the low velocity impact tests; (b) Typical dent geometry created on the flat face of fatigue specimens.

As described in [6], a calibration of the dent depth as a function of the reservoir pressure, and hence the impact velocity, was conducted. From the calibration consistent dent depths were obtained in each experimental damage simulation and different groups of dent depths were generated for the fatigue tests. The geometrical characterisation of the dents was also carried out on an Alicona InfiniteFocus microscope in terms of depth, width and length of the dent. These key dimensions were used in [6] as the validation parameters of the FE model used in to predict the residual stress field around the dent. The specimens were then classified according to the dent

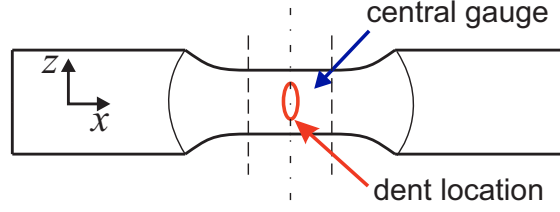


Figure 2: Schematic representation of the fatigue specimen and location of the dent.

depth created, with nominal dent depths of $\sim 25, 50, 127$ and $254 \mu\text{m}$ and a depth tolerance of $\pm 12.7 \mu\text{m}$.

2.2. Fatigue tests

After the surface damage was introduced to the specimens, low cycle fatigue (LCF) tests were conducted by our industrial collaborators at high temperatures, ranging from $600 - 750^\circ\text{C}$. The LCF strain controlled tests were conducted at different strain amplitudes and load ratios of $R = 0$ and $R = -1$. The central gauge of the specimens has a circular cross-section with two flats, the central section has cross-section dimensions of $5 \times 11 \text{ mm}$ and the central gauge length is approximately 14 mm long (Fig. 2). The specimens were shot peened prior to the introduction of the surface damage. Note, however, that the layer of compressive stress generated by the shot-peening is smaller than the last two dent depths analysed [15] and in any case will be significantly modified as a result of the impact. Therefore, the effect of shot-peening on both the damage simulation and the fatigue analysis was neglected. The surface damage was introduced on both sides of the widest side of the cross-section of the specimen, opposite to each other, such that the distance between both dents is $(5 - 2 \times d) \text{ mm}$, where d is the dent depth in mm.

3. Residual stress due low velocity impacts

3.1. Explicit finite element model

Finite element models have been used to simulate various forms of impacts and the residual stress field generated. Boyce et al. [8] investigated the residual stress due to the impact of a spherical projectile on Ti alloys using a quasi-static model. Similarly, Doremus et al. [7] also used a quasi-static indentation model to predict the state of stress around the damage, with reasonably

good accuracy. The argument for the use of quasi-static models is that the velocities in these events are relatively low and, particularly in the case of nickel superalloys, the material is not very strain rate sensitive. Nevertheless, following the work presented in [6, 11], a dynamic model was used here to better compare the numerical results of the impact of hard objects with the experimental damage simulation measurements. The model has been previously validated in [6] by firstly comparing the geometry of the dent with the experimental measurements of the damage geometry. The residual stress field obtained with the model have also been previously validated, but in a volume-averaged manner, since the resolution of the experimental XRD measurements did not allow a direct comparison with the predicted point-wise residual stress components. In the current paper, the results obtained with the same explicit FE model will be compared with *quasi* point-wise FIB-DIC residual stress measurements.

The numerical model was solved using an explicit FE code (LS-DYNA) to simulate the impact of the indenter onto the specimens carried out in laboratory. The model used is shown in Fig. 3, where only one-quarter of the experimental rig was modelled. The material elasto-plastic parameters of the nickel superalloy were provided by our industrial collaborators¹. The only parameter that requires a calibration in the model is the stiffness of the springs, which support the specimen mounting block. These springs are used to model the compliance of the experimental rig during the impact of the striker. The calibration was carried out by comparing the rebound speed in the model, i.e. the speed of the striker after the impact, with the rebound velocities measured with a high speed camera and digital image correlation technique. The optimal value of the spring stiffness was found to be $k = 3 \times 10^3$ N/m and the calibration process, as well as element type and further details about the FE model and material properties, are described in greater detail in [6].

The results obtained with the FE model are presented in Section 3.3 together with a comparison of the stress components σ_{xx} and σ_{yy} with measurements by the FIB-DIC technique.

¹Due to the confidentiality agreement between the University of Oxford and Rolls-Royce plc. we are unable to provide the full material data used in the simulations.

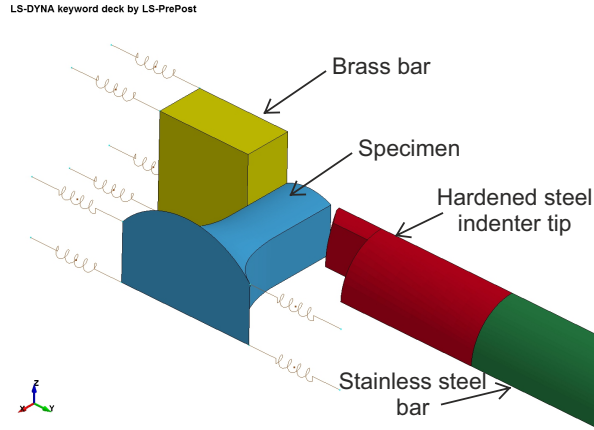


Figure 3: Geometry of the finite element model used in LS-DYNA .

3.2. FIB-DIC measurements

The residual stresses were also measured using a FIB-DIC technique. The FIB-DIC micro-ring core drilling [16, 17] is a promising method for the quantification of the residual stresses at the micron-scale. It allows a “point-wise” description of the stress distribution, since the size of the averaging area is much smaller than the dimension of the dent depth. This contrasts with the averaged measure of stress obtained in the XRD method. Note that the area of the spot size in the XRD measurements in [6] was of the same order of magnitude as the dent depth size. In practice, the area over which stresses are measured in the ring core FIB-DIC technique is smaller than the grain size of the superalloy. This will lead to measurement of inter-granular stress as well as the macroscopic values. These have to be taken into account, as does the anisotropy of single nickel grains. The version of the technique used here employs the use of Focused Ion Beam (FIB) as the means of minimally invasive creation of a circular traction-free trench around the central micro-pillar [18]. The deformation occurring at the pillar top surface is monitored during milling using an SEM, which is integral to the FIB machine. Then Digital Image Correlation (DIC) is used to measure the strain relief of the pillar, or ring core, and this may be directly correlated with the original residual stress field.

The samples were sectioned transverse to the longest axis of the dent (see Fig. 1b) and polished successively down to $0.07 \mu\text{m Ra}$ with a Colloidal Silica solution. The grinding and polishing procedure was designed to minimise residual stress introduced during sample preparation. An Au-

Pd coating of 5 nm thickness was added to the surface of the sample to create a pattern necessary for the DIC analysis. The ring core diameter, D , was set to $5\ \mu\text{m}$ and the final depth of the drilling, H , is also $5\ \mu\text{m}$ Fig. 4a. At each ring core depth, 10 images were captured and averaged to provide an input to the DIC software with low noise. Different depths, h/D , of the ring core are shown in Fig. 5. The images were then used in Matlab-based DIC software, where the strain relief is calculated. Several points under the dent (y direction) were selected for the FIB-DIC procedure, as indicated in Fig. 4b. For each of these points measurements of the residual stress components σ_{xx} and σ_{yy} were obtained, i.e. normal and transverse to the dent root.

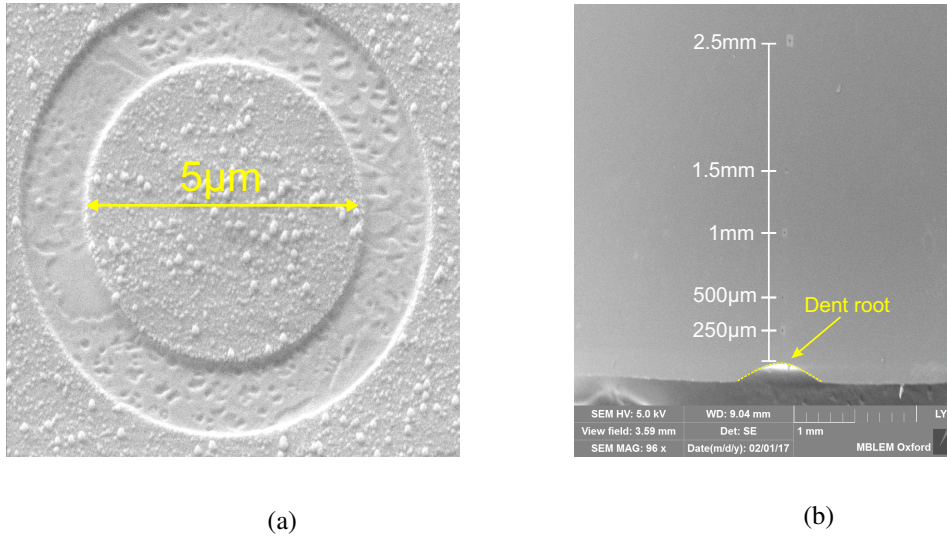


Figure 4: (a) Diameter D of the ring core; (b) and drilling points distance from dent root

3.3. Comparison between predicted and measured residual stresses

As explained above, the residual stress components can be obtained from the measured strain relief of the ring core at each depth [16]. Using a plane stress assumption gives:

$$\begin{aligned}\sigma_{xx} &= \frac{E}{1 - \nu^2} (\epsilon_{xx} + \nu \epsilon_{yy}) \\ \sigma_{yy} &= \frac{E}{1 - \nu^2} (\epsilon_{yy} + \nu \epsilon_{xx})\end{aligned}\tag{1}$$

Note, however, that the stress obtained by the expressions above depends on the bulk elastic

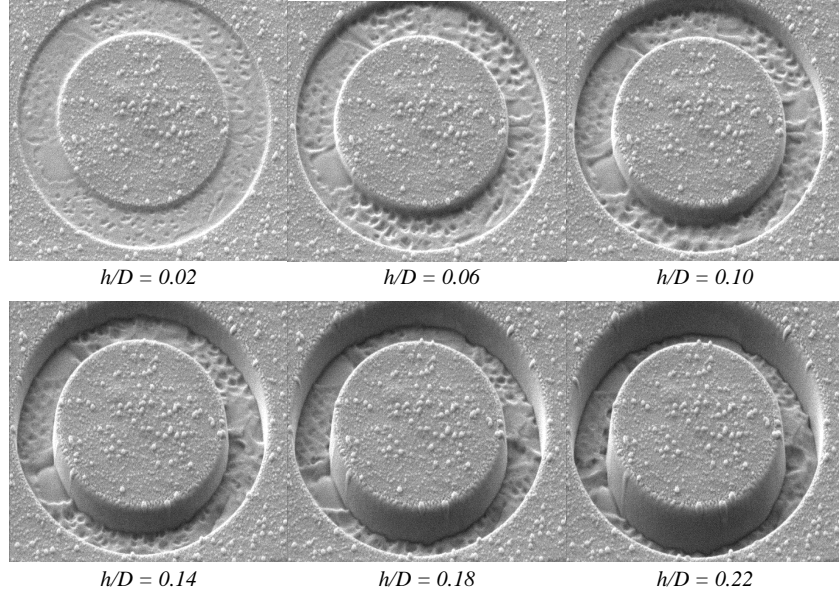


Figure 5: Ring core drilling at different depths h/D .

parameters of the material, when in fact, the size of the ring core is smaller than the nominal grain size of this alloy ($\approx 10 \mu\text{m}$). Hence, for an accurate calculation of the residual stress, one needs to know the orientation of the grain in which the drilling is carried out. The assessment of the error associated with randomly distributed crystal orientations in nickel alloys has been carried out by Salvati et al. [19]. They have shown that the error associated with the grain orientation in nickel alloys is not greater than 40% of the value calculated with the bulk elastic parameters. This uncertainty is therefore represented by error bars in the plots of results.

The residual stress components σ_{xx} and σ_{yy} measured with the FIB-DIC technique are compared in Fig. 6 with predictions of the FE model. Note that the residual stress is affected by the sectioning of the sample. When the stresses normal to sectioned face are released, the components σ_{xx} and σ_{yy} , are redistributed. This is the reason the results presented in Fig. 6 show no compressive zone under the dent. In order to compare the experimental measurements with the FE results, a similar procedure was carried out numerically, i.e. the symmetry boundary conditions were removed in order to emulate the change in stresses due to sectioning of the specimen. The overall trends in the measured and predicted curves show good agreement. The high value of

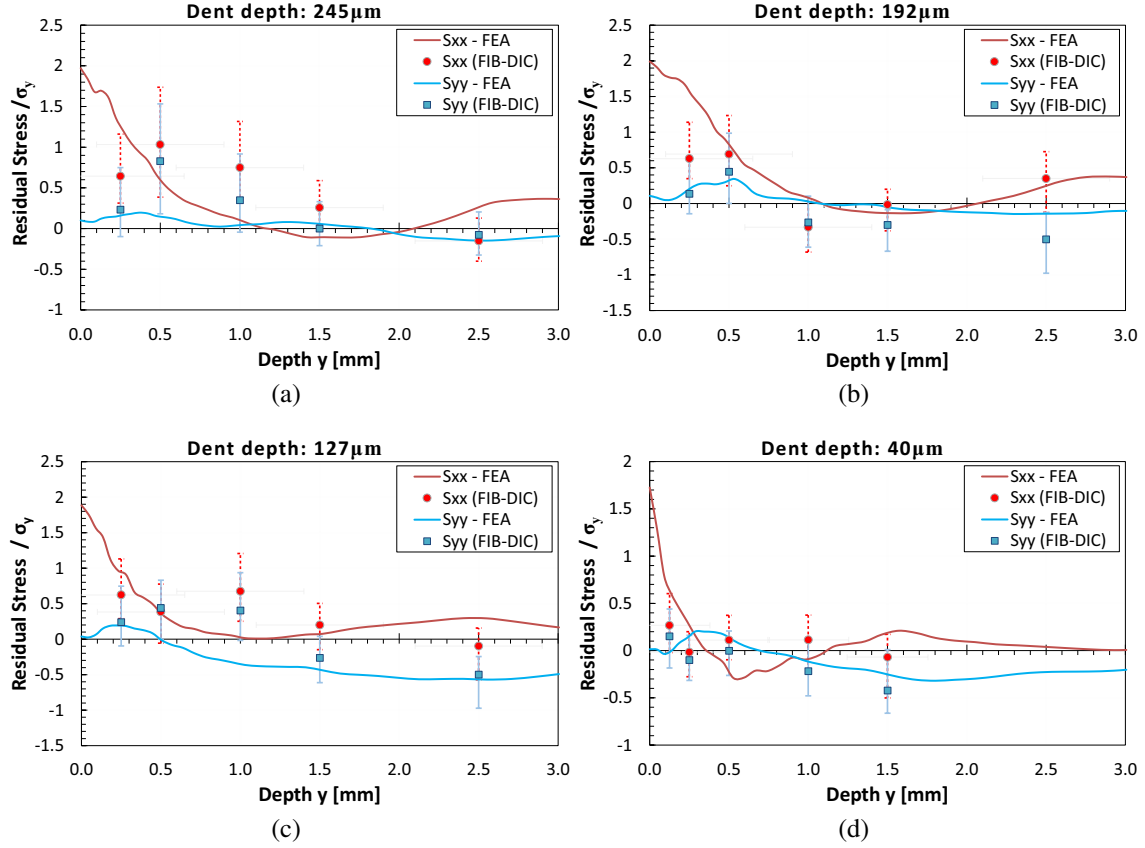


Figure 6: Finite element stress distribution and FIB-DIC measured values, normalised by the room temperature yield stress, for specimens with dent depths of: (a) 246 μm ; (b) 196 μm ; (c) 127 μm ; and (d) 41 μm .

the stress σ_{xx} predicted is due to reverse yielding of the compressive zone under the dent during unloading as the indenter rebounds. In practice, it is likely that some of this high stress will be relaxed in the form of micro cracks near the dented region and this may explain the discrepancy between the FIB-DIC and FE results near the bottom of the dent. The stress component σ_{yy} is normal to the surface and should therefore be zero close to the bottom of the surface, as observed both experimentally and numerically.

4. Residual stress relaxation mechanisms

In the context of handling surface damage, parts and components are generally damaged at room temperature (e.g. during assembly or maintenance). However, service conditions are significantly different, with temperatures reaching between 600 and 750 $^{\circ}\text{C}$ on the rotor discs. Hence,

in order to simulate the operating conditions of engine discs, the fatigue tests were carried out at high temperature. The change in temperature before the start of the fatigue test modifies the material properties, in particular, the yield stress at higher temperatures is reduced. Therefore, some stresses that had not reached yield will now be above the high temperature yield stress, causing further plastic deformation and some residual stress relaxation even before the test starts.

Furthermore, during the fatigue tests, the high residual stress near the bottom of the dent will be relaxed in the first load cycle and possibly subsequently, if the material were to soften. The applied stress during the fatigue tests is added to the pre-existing residual stress field, which may raise the tensile stress near the tip beyond yield, causing further stress relaxation and redistribution. Here, we will only consider the first cycle of loading, which will cause redistribution of the stress profile obtained after the impact simulation. The stress-strain curves for different temperatures were provided by our industrial partner and were used in an implicit quasi-static simulation at the end of the explicit impact simulation.

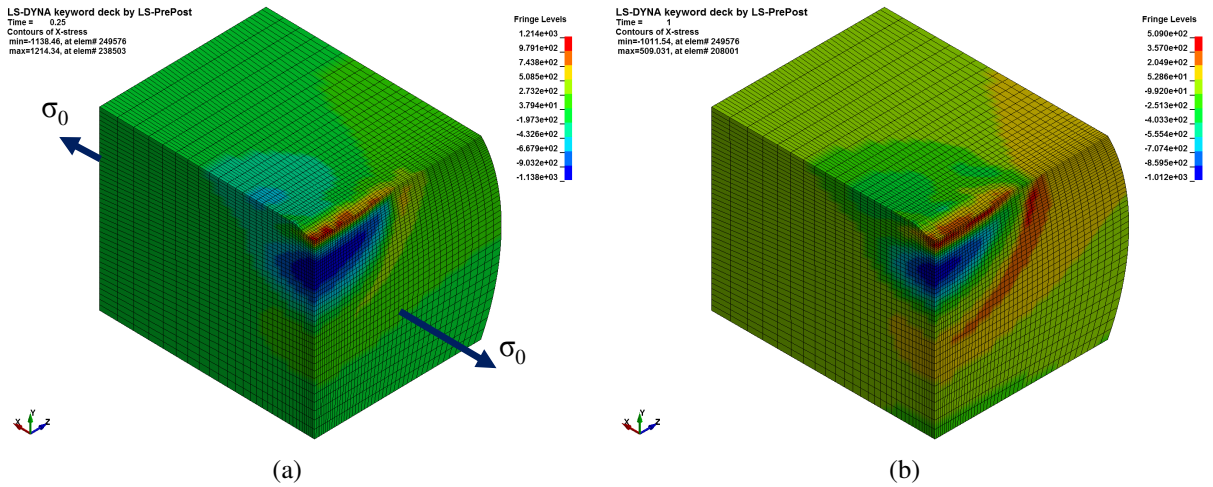


Figure 7: (a) σ_{xx} residual stress field after impact and ; (b) after first load cycle (127 μm dent).

The residual stress relaxation was simulated at the end of the explicit simulation of the impact. A section of the specimen containing the dent was selected and an applied stress σ_0 was applied in the x -direction as shown in Fig. 7a. The material properties for the different temperatures were used in this phase of the analysis. The static analysis was carried out in three steps. First, the equilibrium state of stress was obtained, starting from the output of the dynamic simulation. Then,

a fatigue load was applied monotonically to the specimen up to the maximum value, $\sigma_0 = \sigma_{max}$. Finally, the specimen was unloaded in order to obtain the residual stress state at the end of the first cycle. This procedure was carried out for different temperatures and the difference between the residual stress state before and after the first load cycle is shown in Fig. 7 for a $127 \mu\text{m}$ depth dent.

The effect of both the change in properties due to the increase in temperature and the application of different fatigue loads on the σ_{xx} stress distribution beneath the dent is presented in Fig. 8. It is shown in Fig. 8a the relaxation of residual stress for two different temperatures. In Fig. 8b, the change in residual stress profile for different load levels at 600°C is presented. In both plots, it can be seen that the high tensile stress at the root of the dent is decreased significantly. As a consequence, a redistribution of stresses occurs inside the body and the magnitude of the maximum compressive stress is also reduced. This reduction in magnitude of the compressive stress is important for fatigue life prediction, as the model assumes no crack propagation unless there is a positive stress intensity factor. The effect of negative stress intensity factor on the fatigue life prediction model used has been extensively discussed in [11], where the lack of residual stress relaxation in an earlier model was highlighted as the main reason for the significant divergence between predicted and experimental fatigue lives.

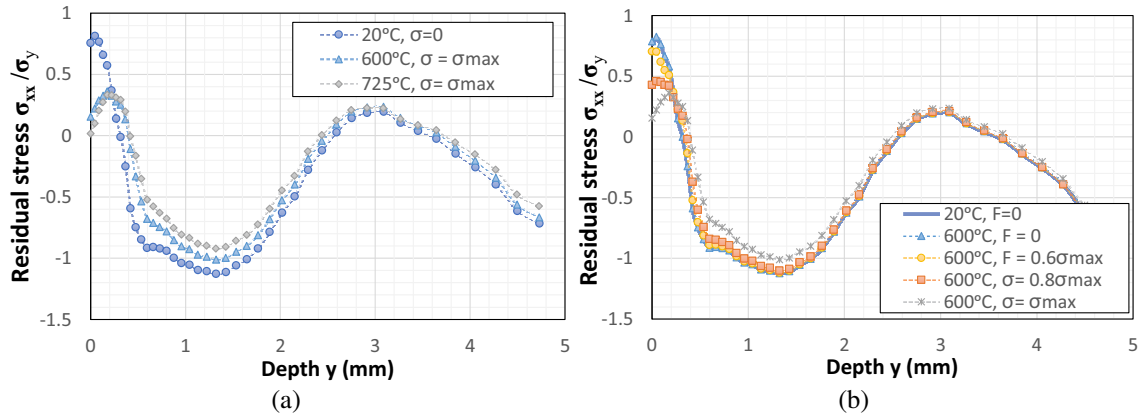


Figure 8: Residual stress relaxation due to (a) temperature; and (b) applied fatigue load ($254 \mu\text{m}$ dents at 600°C).

5. Fatigue crack growth method

5.1. El Haddad model for short cracks

In order to investigate the crack propagation under the dents, a short crack growth model was used. The El Haddad characteristic length was used in [14] to modify the crack length in the stress intensity factor calculation. This approach derives from El Haddad's modification of the the Kitagawa-Takahashi (K-T) diagram by El Haddad et al. [20], and similar methods have been used in [4, 21]. Pugno et al. [22] have suggested a similar method also based on the principle of a modified K-T diagram. The characteristic length was used by El Haddad to obtain a smooth transition between short and long cracks. Using this approach, the corrected effective stress intensity range is given by

$$\Delta K_{eff} = Y \Delta \sigma \sqrt{\pi(a + a_0)}, \quad (2)$$

where a_0 is the El Haddad characteristic length given by the material's fatigue limit, $\Delta \sigma_F$, and the stress intensity factor range threshold, ΔK_0 , as

$$a_0 = \frac{1}{\pi} \left(\frac{\Delta K_0}{\Delta \sigma_f} \right)^2. \quad (3)$$

The effect of adding a_0 to Eq. (2) will be to increase the crack propagation rate substantially in the short crack regime when compared with the traditional Paris law, meaning that cracks will grow below the long crack fatigue threshold, ΔK_0 , provided that a sufficiently high stress range is applied. The fatigue crack growth rate is obtained by substituting ΔK_{eff} in Eq. (2) in the original Paris law, $da/dN = C(\Delta K)^m$, where m and C are parameters obtained experimentally. The final form of the crack evolution equation per cycle can be written in terms of the applied stresses as

$$\frac{da}{dN} = C \left(\Delta K \sqrt{1 + \frac{a_0}{a}} \right)^m, \quad (4)$$

where

$$\frac{a_0}{a} = \left(\frac{\Delta K_0}{\Delta K} \frac{\Delta \sigma}{\Delta \sigma_f} \right)^2. \quad (5)$$

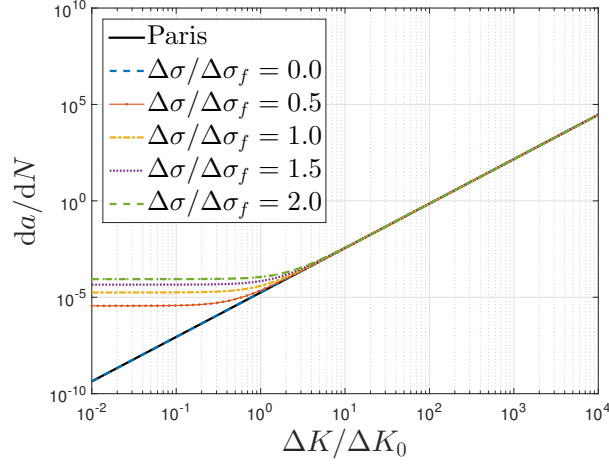


Figure 9: Crack growth law with El Haddad modification for different values of applied load $\sigma/\Delta\sigma_f$.

The crack growth law given by Eq. (4) is shown in Fig. 9 for different ratios of $\Delta\sigma/\Delta\sigma_f$. Despite the simplicity of this method, the crack growth law shows similar results to those observed by experimental measurements [23]. For long cracks, $a \gg a_0$, the effect of the crack length correction is negligible and the predicted crack growth rate is similar to the original Paris law curve of the material.

5.2. Sensitivity to initial crack length

From the short crack growth model given in Eq. (4), the estimated number of cycles for propagation to failure from an initial crack size may be calculated. Note that crack initiation time is not accounted for in the model. For a given stress amplitude, $\Delta\sigma$, the stress intensity factor range, ΔK , is calculated as described above. However, only positive stress intensity factor is considered in this analysis and the range is given by the difference between the maximum K_I calculated and the minimum non-negative K_I . It is, of course, necessary to assume an initial crack length and to choose a critical crack length at which sudden rupture will occur. Due to the exponential crack growth law, the latter does not alter significantly the total crack propagation life predicted and throughout this paper a critical length of $a_c = 2.5$ mm, half the specimen thickness, was assumed. On the other hand, the initial crack length does change considerably the predicted propagation life obtained with a standard Paris law, since the growth rate is much smaller for small ΔK values.

In order to investigate the sensitivity of the proposed method to the choice of initial crack

length, the fatigue life curves, expressed in number of cycles to failure, N_f , as function of applied strain range, obtained for crack lengths varying from 5 – 300 μm are displayed in Fig. 10. For comparison, the characteristic length of the nickel alloy analysed is approximately $a_0 = 100 \mu\text{m}$. For Paris law-driven crack growth rate, a large variation in the fatigue curve is observed with different initial crack lengths. This was expected, as the smaller the initial crack, not only will the crack need to grow a longer distance to reach the critical length, but also its initial growth rate is much smaller due to a smaller ΔK . A lower sensitivity of the modified El Haddad model used here to the initial crack length can also be observed in Fig. 10 (red lines). This is due to the higher crack growth rate for short cracks. Note that only the curve for $a_i = 300 \mu\text{m}$ shows a significant difference with respect to the other initial crack lengths. Here, the initial crack length is already in the long crack region, $a_i > a_0$, and hence the crack growth rate is largely governed by Paris law. For the other initial crack lengths the initial growth rate is essentially the same, i.e. $a_i < a_0$, and hence the change in predicted fatigue life is smaller.

It is also clear from the results in Fig. 10, that once residual stress is included in the calculations (black lines), the overall predicted crack propagation fatigue life is almost independent of the crack initial length. Two properties of the crack growth in the presence of residual stress explain the observed behaviour. The first is given by the fact that the fatigue limit predicted with the model is independent of the choice of initial crack length, it depends only on the maximum compressive residual stress after the relaxation mechanisms, and hence all fatigue curves (dashed-dotted black curves) will converge to the same fatigue limit for lower applied strain ranges. The other reason is that when the initial crack length is small, the crack is in a region of higher tensile stress, hence, a higher ΔK is obtained and the crack growth rate is also higher than in the absence of residual stresses. On the other hand, when a larger initial crack length is given, the initial crack is in a region of lower tensile stresses when compared with smaller initial crack lengths. Therefore, the difference in crack growth rate between the different initial crack lengths is not as accentuated for large applied strains.

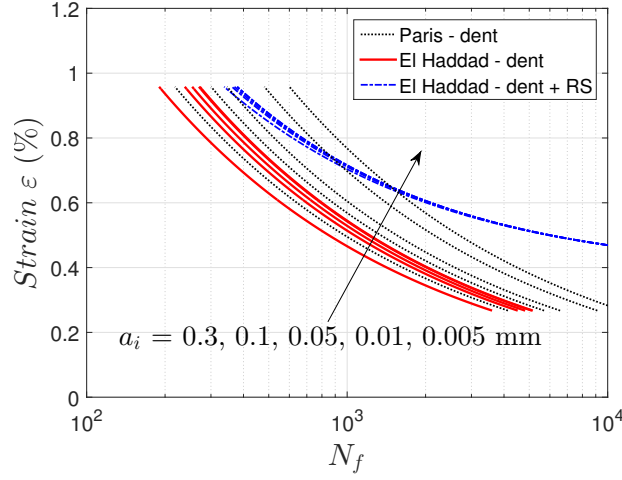


Figure 10: Number of cycles to failure as a function of applied strain range for different initial crack lengths, a_i .

6. Fatigue life analysis

6.1. Stress intensity factors under the dent

The contributions of the dent geometry on the stress intensity factor for a crack growing from the bottom of the dent was calculated for all nominal dent depths tested (Fig. 11). The two-dimensional ‘dislocation density’ method was used for the calculation, as described in [24]. The solution may be compared with both ‘long crack’ and ‘short crack’ limits, and it will be seen that the method correctly reproduces these Fig. 11. The ‘short crack’ bound is given by $K_I = 1.1215K_t\sigma_0\sqrt{\pi a}$, where K_t is the stress concentration factor at the dent root. The ‘long crack’ bound is obtained for large values of a/d , such that, the stress intensity factors will be given by $K_I = 1.1215\sigma_0\sqrt{\pi(a+d)}$ [24]. Note that in this procedure, the stress intensity factor is calculated as a function of the crack length size a/d and the geometry of the dent ρ/d , where ρ is the radius of the bottom of the dent and d is the dent depth. The root radius, ρ , was measured experimentally with an Alicona infinite focus microscope and found to be $\rho = 1.3$ mm for all dent depths. A similar procedure was carried out to calculate the effect of the residual stress field on the stress intensity factor. However, now instead of the applied remote stress σ_0 , the local residual stress field σ_{xx}^r is used in the calculation.

The contribution of the residual stress field to the stress intensity of a crack propagating under the root of dent is shown in Fig. 12. The resultant stress intensity factor is given by the superpo-

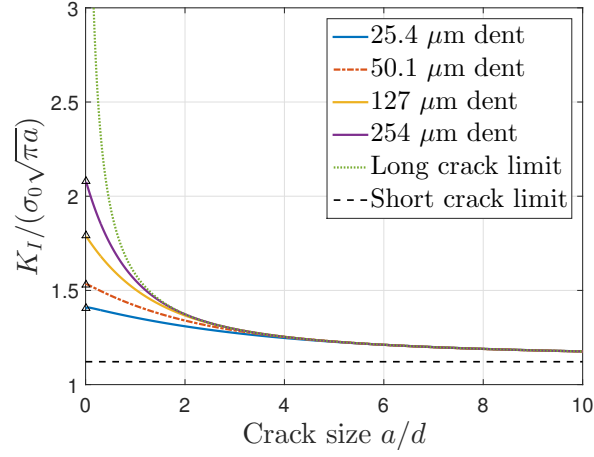


Figure 11: Stress intensity factor due to the notch for a crack propagating under dents of different depths.

sition of the two contributions, i.e. from the residual stress and from the remote fatigue loading. In the fatigue model used here crack growth occurs only for a net positive K_{max} . Hence, in order for propagation to occur, the maximum fatigue load $\sigma_0 = \sigma_{max}$ needs to be sufficient to make the resultant K_I positive, even when the crack enters zones of high compressive residual stress. This condition gives the predicted fatigue limit for the dent and it is the reason it is essential to consider the residual stress relaxation mechanisms discussed.

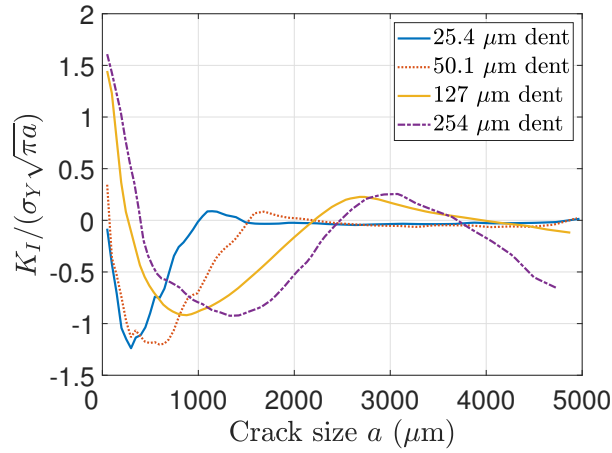


Figure 12: Stress intensity factor due to residual stresses for a crack propagating under dents of different depths.

6.2. Comparison between predicted and experimental results

The crack propagation life predicted with the procedure described here was calculated and compared with experimental results at high temperature. The tests were conducted by the indus-

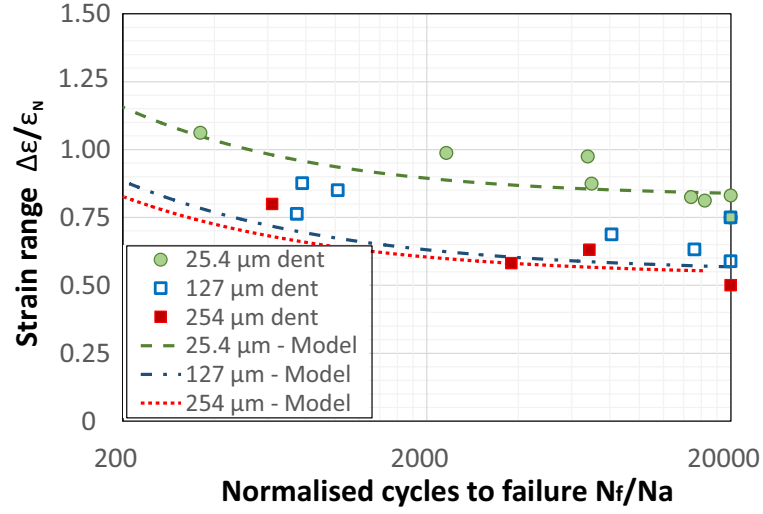


Figure 13: Experimental and predicted number of cycles to failure for different dent depths at 675°C.

trial partner and the objective here is to compare the results with the procedure developed above. The tests used for comparison had a load ratio of $R = 0$. For each temperature level, the appropriate material parameters were used in the calculation of the residual stress relaxation and crack growth analysis. The parameters m and C for the RR1000 nickel superalloy at different temperatures were provided by our industrial collaborator. The predicted curves were obtained by integrating Eq. (4) the residual stress obtained after appropriate relaxation modelling. The predicted fatigue life curves obtained are presented in Figs. 13 and 14 along with experimental results for different dent depths, where the number of cycles to failure, N_f , and the strain range, $\Delta\epsilon$, are normalised by arbitrary constant, N_a and ϵ_N , respectively.

For both temperatures, the predicted and experimental results show a good agreement for the shallowest dent data. It is important to remind the reader that crack initiation time was not regarded in this analysis. Hence, the fact that the curves suggests either that small cracks were generated during the impact of the striker and after application of the fatigue loading, quickly entered a small crack propagation phase, or that the model is in fact underestimating the crack growth rate, but since no initiation time is considered, the results only fortuitously agree. For deeper dents, a disparity between the experimental and predicted curves is observed. This difference was expected due to the absence of initiation time in the model used here. Studies have suggested that initiation and growth of small cracks may account for 80% of the fatigue life [25], without the presence of

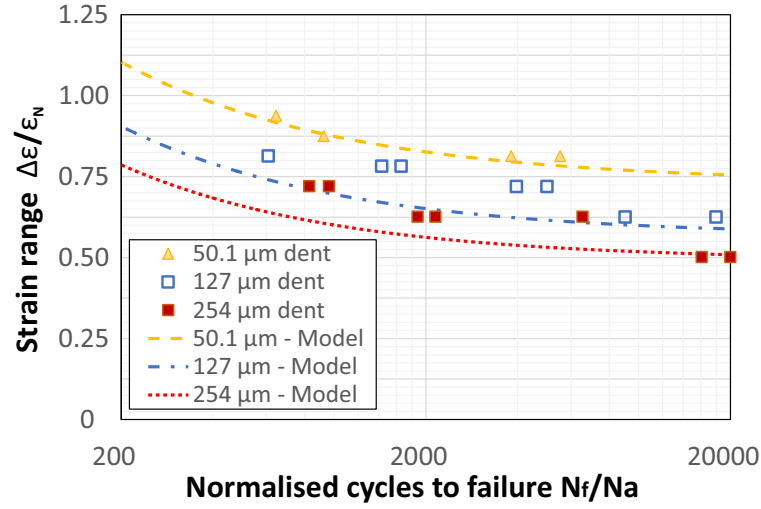


Figure 14: Experimental and predicted number of cycles to failure for different dent depths at 725°C.

residuals stress. Although the latter was accounted for in the model used here, the former was not. However, the region in which the cracks appear, i.e. under the dent root, is a region of tensile residual stress and the time spent on initiation and small crack propagation will likely be reduced here. This change in the proportion of crack initiation on the total fatigue life is also reinforced by the fact that crack growth will slow down when the crack reaches the region of compressive residual stresses. Nevertheless, the difference between experimental and predicted curves may provide a first assessment of the crack initiation time in the fatigue tests with dented specimens.

7. Conclusions

In this work, a comprehensive methodology for evaluating the fatigue life of nickel superalloy parts subject to handling surface damage has been presented. The residual stresses model had been previously validated with XRD measurements, and in this paper a “point-wise” validation of the residual stress distribution was carried out by comparing the results with FIB-DIC core drilling results with some overall agreement in terms of trends between the model and experiment results. It was not surprising that the FIB-DIC measurements did not agree with the numerical model as well as the results obtained with XRD. This is likely to be due to the fact that the model assumes the specimen as an homogeneous isotropic body, while the FIB-DIC measurements are intra-granular. Nevertheless, the overall trend could be captured and it can be observed that the FE

model will over-predict the tensile stresses at the root of the dent in the absence of a model that captures micro damage and cracks at dent the region after impact.

The model developed here demonstrates that a significant improvement in the fatigue life prediction of damaged parts may be obtained by a careful analysis of the residual stress field generated and its changes during operation. Perhaps the most challenging of these analyses is with respect to relaxation mechanisms at play during the fatigue test, and even more so in engine components during operation conditions. In order to improve the calculations of these mechanisms, better material data coupled with more accurate material models, particularly for cyclic alternating elasto-plastic behaviour, are necessary. Only then, can the procedure developed here be applied to alternating load fatigue tests ($R = -1$). Once the residuals stress field was carefully analysed, even with a relatively simple crack growth model used in this work, results were improved with respect to current approaches for crack propagation under handling surface damage. Nevertheless, further improvements are necessary in order to have a reliable and robust model. Particularly, a new modelling approach is needed in order to avoid the high and unrealistic stresses under the dent root. Only then, one may better estimate the crack initiation time under the dents.

8. Acknowledgements

The authors would like to thank Innovate UK and Rolls-Royce plc for the technical and financial support for the work described in this paper.

References

- [1] J. Ding, R.F. Hall, J. Byrne, and J. Tong. Fatigue crack growth from foreign object damage under combined low and high cycle loading. part i: Experimental studies. *Int. J. Fatigue*, 29(7):1339–1349, 2007.
- [2] J. Ding, R.F. Hall, J. Byrne, and J. Tong. Fatigue crack growth from foreign object damage under combined low and high cycle loading. part ii: A two-parameter predictive approach. *Int. J. Fatigue*, 29(7):1350–1358, 2007.
- [3] J.O. Peters, B.L. Boyce, X. Chen, J.M. McNaney, J.W. Hutchinson, and R.O. Ritchie. On the application of the kitagawa–takahashi diagram to foreign-object damage and high-cycle fatigue. *Eng. Fract. Mech.*, 69(13):1425–1446, 2002.
- [4] D. Nowell, P. Duo, and I.F. Stewart. Prediction of fatigue performance in gas turbine blades after foreign object damage. *Int. J. Fatigue*, 25(9):963–969, 2003.

- [5] S. Mall, J. L. Hamrick, and T. Nicholas. High cycle fatigue behavior of ti-6al-4v with simulated foreign object damage. *Mech. Mater.*, 33(11):679–692, 2001.
- [6] R. M. N. Fleury, D. Nowell, T. Sui, S. Ying, A. M. Korsunsky, Y. H. Tai, and F. Silva. Characterisation of handling and service surface damage on nickel alloys caused by low velocity impacts of blunt hard objects. *Mech. Mater.*, 107:45 – 55, 2017.
- [7] L. Doremus, J. Cormier, P. Villechaise, G. Henaff, Y. Nadot, and S. Pierret. Influence of residual stresses on the fatigue crack growth from surface anomalies in a nickel-based superalloy. *Mat. Sci. Eng. A-Struct.*, 644:234–246, 2015.
- [8] B.L. Boyce, X. Chen, J.W. Hutchinson, and R.O. Ritchie. The residual stress state due to a spherical hard-body impact. *Mech. Mater.*, 33(8):441–454, 2001.
- [9] S. Gourdin, L. Doremus, Y. Nadot, G. Hénaff, and S. Pierret. Fatigue crack growth from handling surface anomalies in a nickel based superalloy at high temperature. In *MATEC Web of Conferences*, volume 14, page 16003. EDP Sciences, 2014.
- [10] S. Gourdin, J. Cormier, G. Henaff, Y. Nadot, F. Hamon, and S. Pierret. Assessment of specific contribution of residual stress generated near surface anomalies in the high temperature fatigue life of a rené 65 superalloy. *Fatigue Fract. Eng. M.*, 2016.
- [11] R. M. N. Fleury and D. Nowell. Evaluating the influence of residual stresses and surface damage on fatigue life of nickel superalloys. *Int. J. Fatigue*, 105:27 – 33, 2017.
- [12] D Nowell and DA Hills. Open cracks at or near free edges. *J. Strain Anal. Eng.*, 22(3):177–185, 1987.
- [13] D Nowell. Strain changes caused by finite width slots, with particular reference to residual stress measurement. *J. Strain Anal. Eng.*, 34(4):285–294, 1999.
- [14] S.Y. Oakley and D. Nowell. Prediction of the combined high-and low-cycle fatigue performance of gas turbine blades after foreign object damage. *Int. J. Fatigue*, 29(1):69–80, 2007.
- [15] S. Wang, Y. Li, M. Yao, and R. Wang. Compressive residual stress introduced by shot peening. *J. Mater. Process. Tech.*, 73(1):64 – 73, 1998.
- [16] A. M. Korsunsky, M. Sebastiani, and E. Bemporad. Focused ion beam ring drilling for residual stress evaluation. *Mat. Lett.*, 63(22):1961–1963, 2009.
- [17] E. Salvati, S. O’Connor, T. Sui, D. Nowell, and A. M. Korsunsky. A study of overload effect on fatigue crack propagation using ebsd, fib–dic and fem methods. *Eng. Fract. Mech.*, 167:210–223, 2016.
- [18] E. Salvati, T. Sui, A. J. G. Lunt, and A. M. Korsunsky. The effect of eigenstrain induced by ion beam damage on the apparent strain relief in fib–dic residual stress evaluation. *Mater. Desing*, 92:649–658, 2016.
- [19] E. Salvati, T. Sui, and A. M. Korsunsky. Uncertainty quantification of residual stress evaluation by the fib–dic ring-core method due to elastic anisotropy effects. *Int. J. Solids Struct.*, 87:61–69, 2016.
- [20] MH El Haddad, TH Topper, and KN Smith. Prediction of non propagating cracks. *Eng. Fract. Mech.*, 11(3):573–

584, 1979.

- [21] P Duo, D Nowell, and J Schofield. Assessment of foreign object damage (fod) to aero engine blades. In *Proceeding of the 9th National Turbine Engine HCF Conference, Pinehurst, NC*. Citeseer, 2004.
- [22] N. Pugno, M. Ciavarella, P. Cornetti, and A. Carpinteri. A generalized paris law for fatigue crack growth. *J. Mech. Phys. Solids*, 54(7):1333–1349, 2006.
- [23] A. de Pannemaecker, J. Y. Buffiere, S. Fouvry, and O. Graton. In situ fretting fatigue crack propagation analysis using synchrotron x-ray radiography. *Int. J. Fatigue*, 97:56–69, 2017.
- [24] D. Nowell, D. Dini, and P. Duó. Stress analysis of v-notches with and without cracks, with application to foreign object damage. *J. Strain Anal. Eng.*, 38(5):429–441, 2003.
- [25] G. Socha. Experimental investigations of fatigue cracks nucleation, growth and coalescence in structural steel. *Int. J. Fatigue*, 25(2):139 – 147, 2003.